JACS
JOURNAL OF THE AMERICAN CHEMICAL SOCIETY
Article
pubs.acs.org/JACS

Conformational Transition and Energy Landscape of ErbB4 Activated by Neuregulin1β: One Microsecond Molecular Dynamics Simulations

Yun Du, Huaiyu Yang,* Yechun Xu, Xiaohui Cang, Cheng Luo, Yanyan Mao, Yuanyuan Wang, Guangrong Qin, Xiaomin Luo, and Hualiang Jiang*

Drug Discovery and Design Center, State Key Laboratory of Drug Research, Shanghai Institute of Materia Medica, Chinese Academy of Sciences, 555 Zuchongzhi Road, Shanghai 201203, China

Supporting Information

ABSTRACT: ErbB4, a receptor tyrosine kinase of the ErbB family, plays crucial roles in cell growth and differentiation, especially in the development of the heart and nervous system. Ligand binding to its extracellular region could modulate the activation process. To understand the mechanism of ErbB4 activation induced by ligand binding, we performed one microsecond molecular dynamics (MD) simulations on the ErbB4 extracellular region (ECR) with and without its endogenous ligand neuregulin1β (NRG1β). The conformational transition of the ECR-ErbB4/NRG1β complex from a tethered inactive conformation to an extended active-like form has been observed, while such large and function-related conformational change has not been seen in the simulation on the ECR-ErbB4, suggesting that ligand binding is indeed the active inducing force for the conformational transition and further dimerization. On the basis of MD simulations and principal component analysis, we constructed a rough energy landscape for the conformational transition of ECR-ErbB4/NRG1β complex, suggesting that the conformational change from the inactive state to active-like state involves a stable conformation. The energy barrier for the tether opening was estimated as ~2.7 kcal/mol, which is very close to the experimental value (1−2 kcal/mol) reported for ErbB1. On the basis of the simulation results, an atomic mechanism for the ligand-induced activation of ErbB4 was postulated. The present MD simulations provide a new insight into the conformational changes underlying the activation of ErbB4.

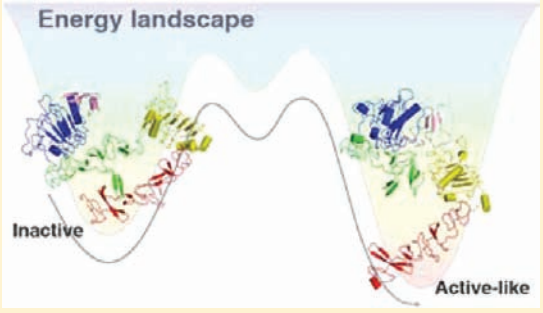

INTRODUCTION

The ErbB family receptor tyrosine kinases consist of four members, epidermal growth factor receptor (ErbB1/EGFR), ErbB2 (HER2), ErbB3 (HER3), and ErbB4(HER4), all of which play fundamental roles in regulating cell proliferation and differentiation.[1] Members of this family share a similar structural arrangement and activation mechanism. Each member consists of an extracellular region, a single transmembrane-spanning region, a cytoplasmic tyrosine kinase domain, and a carboxyl terminal domain.[2] Ligand binding to the extracellular region promotes activation and dimerization of ErbB receptors, leading to activation of their intracellular parts and thereby further triggering downstream pathways such as those centered on MAPK or PI3K.[3] Because of their important biological and pharmacological functions, ErbBs have been extensively studied as drug targets.[4]

ErbB4 is the most recently characterized member of the ErbB family and has been shown to be essential in the development of nervous and cardiovascular systems.[5−7] Loss of function of the ErbB4 gene has been implicated in the pathology of diseases such as schizophrenia[8−10] and heart failure.[11] However, the role of ErbB4 in oncogenesis is far from clear; whether it is a tumor suppressor[12−17] or an oncogene[18−23] is still under debate. As the initiation step of an entire signaling cascade, abnormal ErbB4/ligand interactions in the extracellular region may take crucial roles in these pathogenic mechanisms. Accordingly, it is of particular importance to investigate the dynamic properties of ErbB4 extracellular region and its ligand-binding properties.[24]

The neuregulin (NRG) family growth factors are endogenous ligands of ErbB4.[25] As the best characterized member, NRG1 has different variants of EGF-like domains (α and β), which differ in affinity to ErbB4. Also, the isolated EGF-like domain has been demonstrated to be necessary and sufficient for NRG1 to bind to and activate ErbB4.[26] Accordingly, this peptide ligand, the EGF-like domain of NRG1, has been widely used for studying the activation of ErbB4.

As limited structural information was obtained about ErbB4,[25] relevant data for other homologues in the ErbB family are helpful in understanding the activation of the ErbB4 extracellular region (ECR). This region is composed of four domains arranged as tandem repeats of a leucine-rich domain (domains I and III) and a cysteine-rich domain (domains II and IV).[25] The currently available crystal structures of the ECRs of ErbBs comprise four states, that is, "unliganded-inactive",

Received: December 22, 2011
Published: February 8, 2012

   dx.doi.org/10.1021/ja211941d | J. Am. Chem. Soc. 2012, 134, 6720−6731

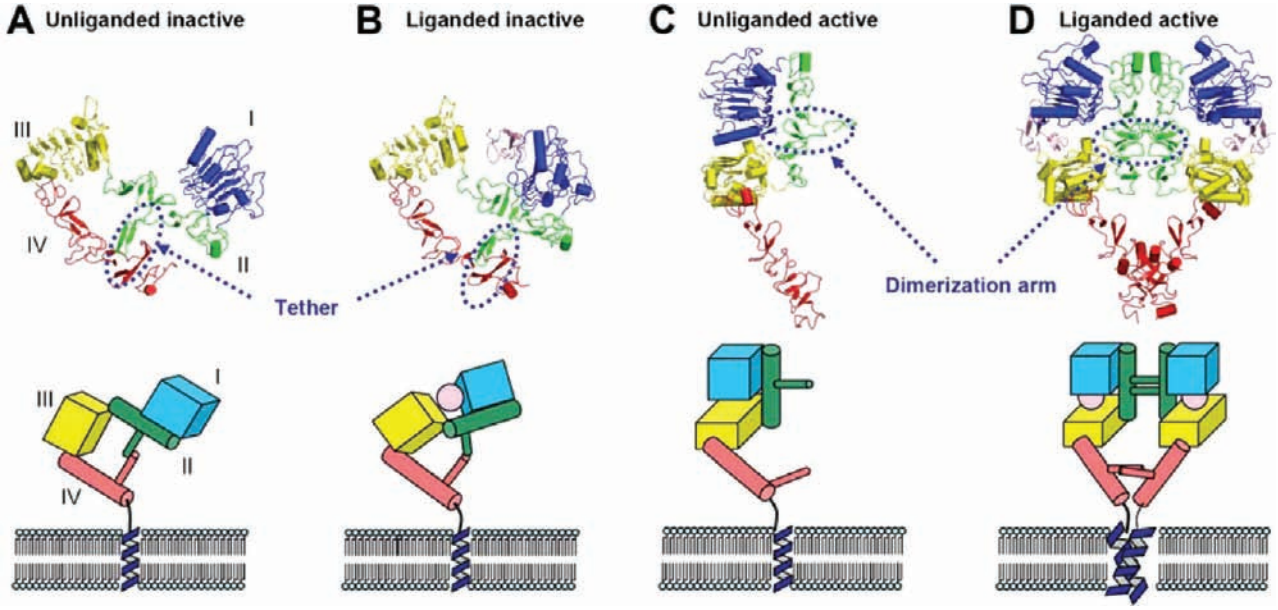

Figure 1. Crystal structures for the extracellular regions (ECRs) of ErbB family members. (A) Unliganded-inactive ECR-ErbB4 monomer (PDB code: 2AHX). (B) Liganded-inactive ECR-ErbB1/EGF complex monomer (PDB code: 1NQL). (C) Unliganded-active ECR-ErbB2 monomer (PDB code: 3N85). (D) Liganded-active ECR-ErbB1/EGF complex dimer (PDB code: 3NJP). The ligand and domains I–IV of ErbBs are colored in pink, blue, green, yellow, and red, respectively. The cartoon representations of the ECRs of ErbBs together with their single transmembrane regions and lipid bilayer are displayed below the structures.

"liganded-inactive", "unliganded-active", and "liganded-active" (Figure 1). The three-dimensional (3D) structure of the ECR of ErbB4 has been determined only as an unliganded-inactive state, which adopts the architecture similar to the unliganded-inactive ErbB1 and ErbB3.[25,27,28] The intramolecular domain II/IV contact (also known as the "tether" structure) buries the "dimerization arm", a β-hairpin loop located on domain II, thereby preventing the formation of dimers (Figure 1A). Being the only liganded-inactive structure reported to date,[29] the ErbB1/EGF 1:1 complex adopts a similar "tethered" conformation with ligand binding exclusively to domain I (Figure 1B). The unliganded-active structure is found only in ErbB2, a unique receptor in the ErbB family because of its ligand-independent activation. Without ligand binding, the active ErbB2 adopts an extended conformation,[30,31] in which the dimerization arm is constitutively exposed (Figure 1C). The liganded-active dimers of ErbB1 are characterized by intermolecular contacts between the dimerization arms of the two monomers (Figure 1D). In the crystal structures identified earlier, domain IV is not visible in the electron density map.[32,33] Nevertheless, the results of the small-angle X-ray scattering (SAXS) experiment on the isolated ECR-ErbB1 indicate a mutual orientation of domains III and IV that is similar to what has been found in the inactive monomer.[34] A recently reported ErbB1/EGF structure in dimeric form comprising domains I–IV of the complete ECR[35] further supported the presumed architecture of active dimer. Although the structure of ErbB4 has only been determined in the unliganded-inactive state, other states, especially the liganded-active state, are highly probable for ErbB4 because the receptor has been shown to resemble ErbB1 in its ability to form ligand-dependent homodimers in solution and on the cell surface.[25]

Although the crystal structures provide snapshots of probable inactive and active conformations of ErbB4, they do not explain the exact activation mechanism.[36] It has been generally assumed that ligand binding to ErbBs, including ErbB4, shifts the monomer–dimer equilibrium in favor of the dimeric state. However, it is still unclear whether the ligand shifts the spontaneous conformational transition equilibrium of ErbB4 by trapping the receptor molecule in the active state ready for dimerization or the ligand binds to and promotes a dramatic conformational change of the receptor, so that the tether is opened and the dimerization arm becomes exposed for dimer formation. To answer those fundamental questions, we have performed microsecond (μs) scale molecular dynamics (MD) simulations on the extracellular region of ErbB4 (simply called ECR-ErbB4 hereafter) in both unliganded and liganded states. In the following, we report on the MD simulation results for the conformational transition mechanism of ErbB4 from the inactive state to an "active-like" state.

METHODS

Starting Structures for Simulations. Coordinates of ECR-ErbB4 (residues 29–641) were taken from a crystal structure (PDB code: 2AHX).[25] The coordinates of residues missing due to lack of interpretable electron density (residues 181–184 and 327–329) were generated by the loop-search method included in the Homology module of Insight II (Accelrys, Inc., San Diego, CA). The 3D structure of the ligand, the EGF-like domain in neuregulin1β (NRG1β) (residues 177–229), was constructed by homology modeling based on the NMR coordinates of neuregulin1α (NRG1α) (PDB code: 1HAF)[37] as reported in our previous work.[38]

Subsequently, four simulation systems were designed based on the structures of ECR-ErbB4 and the ligand NRG1β. For the first simulation, the starting conformation comprised an ECR-ErbB4 and a free ligand which was located in the gap between domains I and III of ErbB4. The second simulation started with an unliganded ECR-ErbB4. The third simulation started with the complex of ECR-ErbB4/NRG1β in which ligand NRG1β was bound to domain I of ErbB4. The complex was constructed by using an inactive ECR-ErbB1/EGF complex (PDB code: 1NQL)[29] as reference. The starting structure of the fourth simulation was the same as the third simulation system except that K181, K187, and R220 of the ligand were mutated into glutamates.

dx.doi.org/10.1021/ja211941d | J. Am. Chem. Soc. 2012, 134, 6720–6731

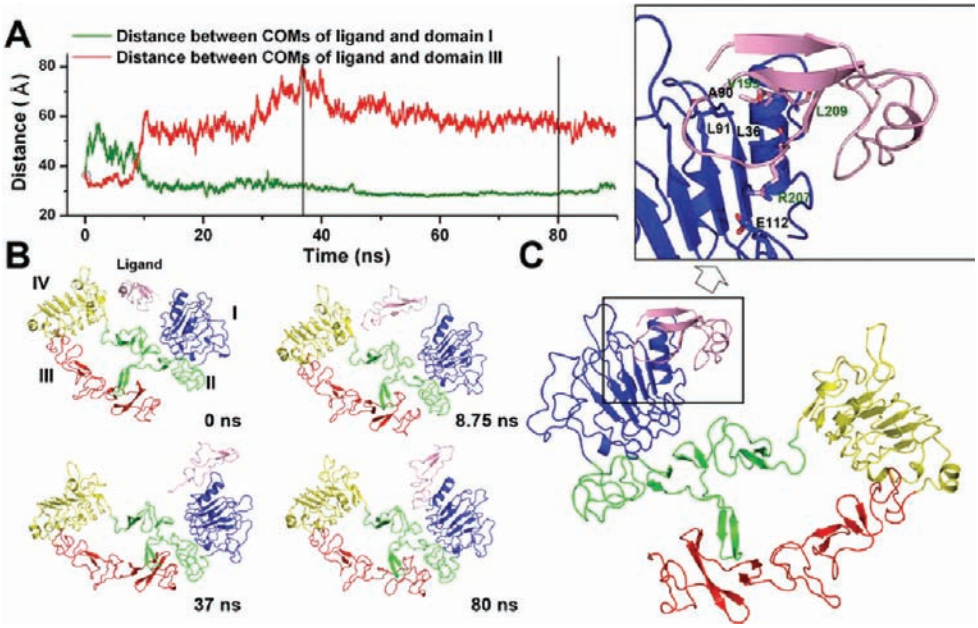

Figure 2. Preliminary simulation result for the binding between ECR-ErbB4 and NRG1β. (A) Time dependence for COM distances of NRG1β with domains I (green curve) and III (red curve) of ErbB4. (B) Typical snapshots taken from the MD trajectory for the simulation concerning binding between ECR-ErbB4 and NRG1β. (C) Homology modeled initial structure of inactive ECR-ErbB4/NRG1β complex for long-time MD simulation. The details of receptor/ligand interactions are shown on the top. Residues from ECR-ErbB4 contributing to the binding are labeled in black, and those from NRG1β are labeled in green. For all of the structures, NRG1β and domains I–IV of ECR-ErbB4 are colored in pink, blue, green, yellow, and red, respectively.

MD Simulations. MD simulations were carried out with the GROMACS 4 package[39,40] using the NPT ensemble and periodic boundary condition. The Amber Parm99 force field[41,42] was applied to the protein or protein complex by using scripts provided by ANTECHAMBER/GAFF-ffamber port.[43] In each simulation, the protein or protein complex was solvated in a box with TIP3P water molecules,[44] keeping the boundary of the box at least 10 Å away from any protein atoms. The resulting system was then submitted to energy minimization. Counterions were subsequently added for charge neutralization. Energy minimization was then repeated on the whole system. After convergence had been reached, the solvent, the counterions, and the protein or protein complex were sequentially coupled to a temperature bath at 310 K with a coupling time of τ_T = 0.1 ps by the Berendsen thermostat.[12,13] The pressure was maintained at 1 bar by using the Berendsen barostat with τ_p = 1.0 ps and a compressibility of 4.5 × 10^{-5}/bar.[45] Electrostatic interactions were calculated using the particle mesh Ewald (PME) algorithm.[46,47] The LINCS method[48] was used to restrain bond lengths, including hydrogen atoms, allowing an integration step of 2 fs. The coordinates of the whole system were saved every 10 ps.

Curvature of Domain II Calculation. The domain II of ECR-ErbB4 shows a "spine-like" structure,[25] which is composed of seven laminin-like modules organized in a C2–C2–C1–C1–C1–C1–C1 sequence (a module defined by a single disulfide bond is called C1, and one defined by two intertwined disulfides that link the side chains in a pattern of Cys1–Cys3 and Cys2–Cys4 is called a C2 module). The "spine" can bend because of the relative movements between these laminin-like modules. The position of each module could be represented by the center of mass (COM) of the sulfur atoms forming disulfide bonds within it. Then the seven COMs are used to fit a curve. The maximum curvature of the curve represents the bending of the domain. Polynomial regression (with the function of $f(x) = c_0 + c_1x + c_2x^2$) was employed to obtain the fitted curve. Then curvature was calculated with eq 1:

$$\kappa = \frac{(1 + f'^2(x))^{1/2} f''(x)}{(1 + f'^2(x))^2} \quad (1)$$

Electrostatic Potential Calculation. The electrostatic potential mapped onto the solvent-accessible surface was calculated using the PDB2PQR software[49,50] and the APBS program.[51] The results were presented with PyMOL,[52] and the potential is scaled to ±5 k_BT/e, where k_B is the Boltzmann constant, T is the temperature, and e is the charge of an electron.

Principle Component Analysis. Principle component analysis (PCA)[53] was carried out to address the collective motions of ECR-ErbB4/NRG1β complex by using the positional covariance matrix C of the atomic coordinates and its eigenvectors. The elements of the positional covariance matrix C are defined by eq 2:

$$C_i = \langle (x_i - \langle x_i \rangle)(x_j - \langle x_j \rangle) \rangle \; (i, j = 1, 2, 3, ..., 3N) \quad (2)$$

where x_i is the Cartesian coordinate of the ith C_α atom, N is the number of C_α atoms considered, and $\langle x_i \rangle$ represents the time average over all of the configurations obtained in the simulation. The eigenvectors of the covariance matrix, V_k, obtained by solving $V_k^T C V_k = \lambda_k$, stand for a set of 3N-dimensional directions, or principal modes, along which the fluctuations observed in the simulation are uncoupled with respect to each other and can be analyzed separately.

Energy Landscape Analysis. The energy landscape for the conformational change of a protein or protein complex can be obtained by an appropriate conformational sampling method. Conformations produced by MD simulations were used for energy analysis in this study. To obtain a two-dimentional (2D) representation of the energy landscape, the distance between the COMs of domains II and IV, which mainly corresponded to the motion of principle component 1 (PC1), and the cleft angle between the domain I/II pair and the domain III/IV pair, which matched the motion of principle component 2 (PC2), were selected as reaction coordinates. The energy landscape along these two reaction coordinates could be obtained by eq 3:[54–56]

$$G(q_1, q_2) = -k_B T \ln P(q_1, q_2) \quad (3)$$

where k_B is the Boltzmann constant, T is the temperature of simulation, and $P(q_1,q_2)$ is the normalized joint probability distribution. The energy surface obtained from the raw data was

dx.doi.org/10.1021/ja211941d | J. Am. Chem. Soc. 2012, 134, 6720–6731

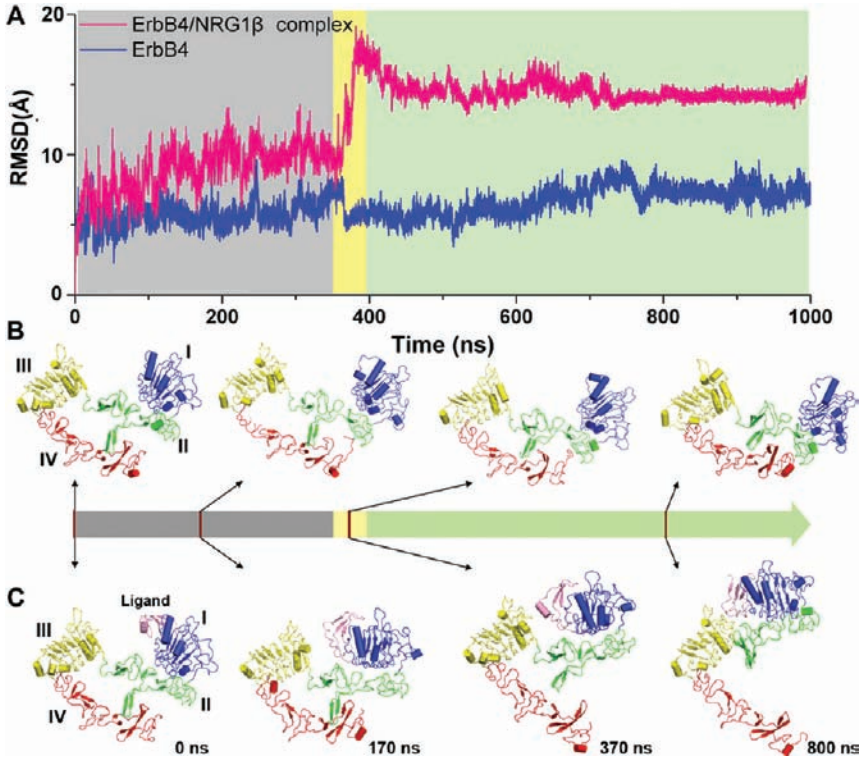

Figure 3. Motions of ECR-ErbB4 in the presence and absence of the ligand NRG1β. (A) Backbone rmsd values of the unliganded (blue) and liganded (pink) ECR-ErbB4 versus simulation time. Three stages for the liganded ErbB4 conformational change are denoted with the background colored in gray, light yellow, and light green. (B) Snapshots extracted from the 1 μs MD simulation trajectory on ECR-ErbB4 in the absence of ligand. (C) Snapshots of ECR-ErbB4/NRG1β complex extracted from the 1 μs MD simulation trajectory. NRG1β and domains I–IV are colored in pink, blue, green, yellow, and red, respectively.

further smoothed by using the kernel density smooth method encoded in the fields module[57] of the R program,[58] and the graphic views were generated with the RGL module[59] of the R program.[58]

Of note, in general, eq 3 could not be used to calculate the free-energy landscape with only unidirectional MD trajectory from the inactive state to the active state because the distribution obtained from the trajectory might not be an equilibrium one. Nevertheless, it seems that the conformational transition of ECR-ErbB4/NRG1β takes place along a pathway near the equilibrium one because of following observations: (*i*) the tether opening process of ECR-ErbB4/NRG1β might be relatively slow, taking ~400 ns in the MD simulation; (*ii*) the MD trajectory of ECR-ErbB4/NRG1β addressed a similar structure for the ECR-ErbB1/EGF complex determined by crystallography;[29] and (*iii*) the estimated energy barrier for the conformational transition of ECR-ErbB4/NRG1β happened to be close to the experimental value reported for ErbB1. Accordingly, we used eq 3 to estimate the energy landscape for the conformational transition.

RESULTS

Neuregulin1β (NRG1β) Initially Binds to Domain I of ErbB4. Because the experimental 3D structure of neuregulin1β (NRG1β), a high-affinity endogenous ligand of ErbB4, is not available, we constructed a 3D model for this ligand by homology modeling based on the NMR structure of the EGF-like domain of the neuregulin1α (NRG1α) (PDB code: 1HAF),[37] a ligand highly similar to NRG1β. Moreover, since only the unliganded-inactive structure is available for ECR-ErbB4 (PDB code: 2AHX),[25] we had to build a rational starting structure of the ECR-ErbB4/NRG1β complex for further MD simulations. The crystal structure of the liganded-active ECR-ErbB1/EGF complex (PDB codes: 1IVO, 1MOX and 3NJP)[32,33,35] revealed that ligand binding with both domains I and III is an important feature of the active conformations of ErbBs (Figure 1D). Consequently, a question arises concerning the initial stage of ErbB4 activation: Is NRG1β trapped selectively by some specific conformations along the conformational change pathway of ErbB4, or does it actively bind to domain I or domain III first before it triggers ErbB4 to undergo a conformational transition?[36] The first option has been rejected by a 1 μs MD simulation on the unliganded ErbB4 (see the results below). Meanwhile, to tentatively validate the possibility of the second option, we performed a 90 ns MD simulation on a model of the inactive ECR-ErbB4 and NRG1β, in which the ligand NRG1β was placed in the middle of the gap between domains I and III of ErbB4. The result reveals that the ligand moves quickly toward domain I and binds to the domain at ~12 ns (Figure 2A,B), implying that in the very beginning of the whole activation process, NRG1β tends to bind to domain I rather than domain III of the tethered ErbB4. Although domains I and III are highly homologous, their ligand-binding surfaces are quite different.[36] The contact area for ligand on domain I is larger than that on domain III as indicated by the liganded-active crystal structures of ErbB1.[32,33,35] This might be the major reason for NRG1β to contact domain I before it initiates the conformational change of ErbB4. Our simulation result is also in agreement with the X-ray structure of the inactive ECR-ErbB1/EGF complex (PDB code: 1NQL), in which EGF binds exclusively to domain I rather than domain III (Figure 1B).[29]

Our 90 ns MD simulation also revealed some primary hints for the ErbB4 activation. During the simulation, NRG1β departed away from domain III in the beginning ~40 ns; soon afterward, however, it tended to move to domains III again

dx.doi.org/10.1021/ja211941d | J. Am. Chem. Soc. 2012, 134, 6720–6731

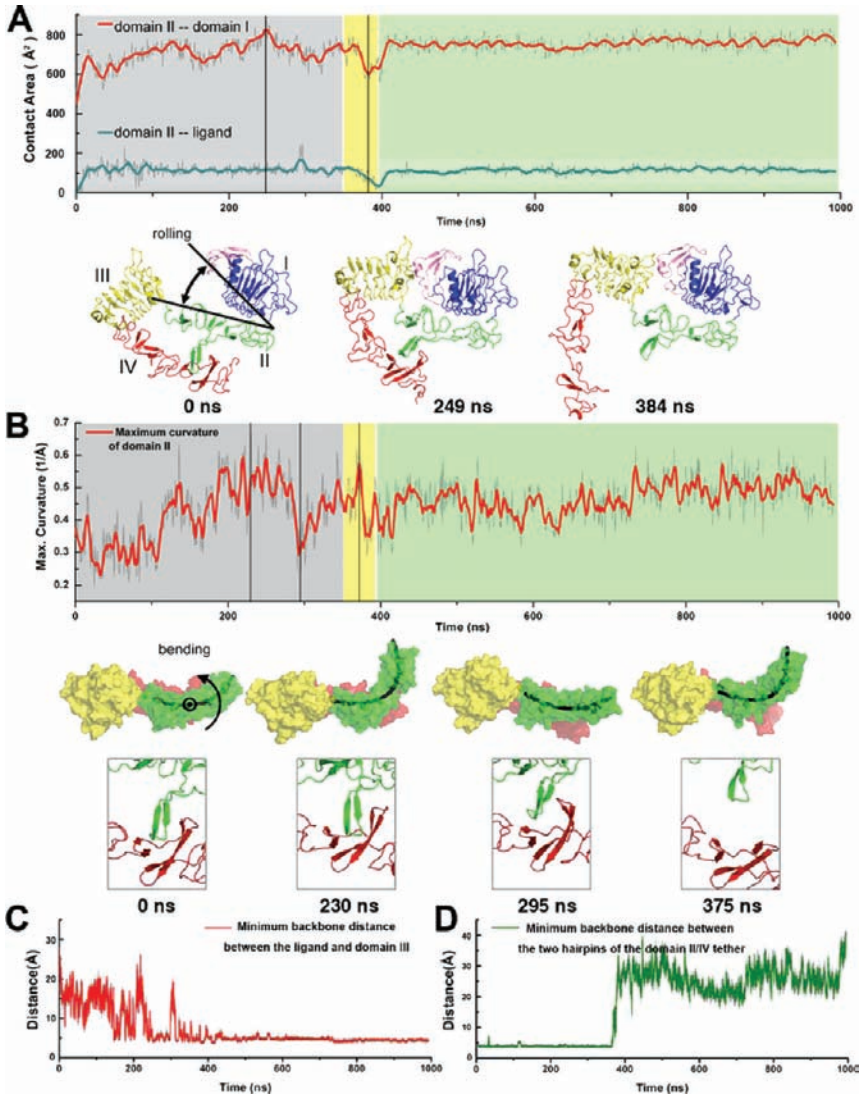

Figure 4. Dynamic features of the conformational change for the ECR-ErbB4/NRG1β complex. (A) Rolling motion of domain I and ligand. Time evolutions of contact areas of the domains I/II pair and ligand/domain II pair are shown on the top. The snapshots at 0, 249, and 384 ns are shown on the bottom. This rolling motion is denoted on the 0 ns conformation, with the arrow indicating the rolling direction. (B) Bending vibration of domain II. Time evolution of maximum curvature of domain II is shown on the top. The snapshots at 0, 230, 295, and 375 ns are shown in the middle. The black lines are the fitted curves representing the bending of domain II. This bending motion is illustrated on the 0 ns conformation, in which the circle indicates the axis of rotation and the arrow indicates the direction of bending. The related process of tether loosening and rupture is shown at the bottom. (C) Time evolution of the minimum backbone distance between ligand and domain III. (D) Time evolution of the minimum backbone distance between two hairpin protrusions on domains II and IV, which form the domain II/IV tether. For all of the representations of time evolutions, the raw data are shown in gray. The adjacent averaging method is employed to get the smoothed curves (25 data points at a time are considered by the smoothing routine), and the smoothed curves are shown in red or green.

(Figure 2A). This result implies that the ligand may pull domains I and III to move together after tightly binding to domain I. This primary idea has been confirmed by the following 1 μs MD simulations (see the following results).

With the knowledge that NRG1β binds to domain I of ErbB4 before it initiates the receptor activation, we constructed a more appropriate model of the inactive ECR-ErbB4/NRG1β complex for further long-time-scale MD simulations. On the basis of the homology between ErbB4 and ErbB1, and the structural similarity between NRG1β and EGF, a ligand of ErbB1,[25] a 3D structural model of inactive ECR-ErbB4/NRG1β complex was constructed by using the crystal structures of the inactive ErbB1/EGF complex (PDB code: 1NQL), ErbB4 (PDB code: 2AHX), and the model of NRG1β. The 3D model of ECR-ErbB4/NRG1β complex was built by superimposing the crystal structure of ErbB4 and the NRG1β 3D model, respectively, with the coordinates of ErbB1 and EGF in the inactive ECR-ErbB1/EGF complex, and then the structural model was optimized using the Amber Parm99 force field.[37,38] The final 3D model is shown in Figure 2C.

NRG1β Induces Conformational Changes of ErbB4. One microsecond MD simulations were carried out on both the crystal structure of inactive-unliganded ECR-ErbB4 and the 3D model of the inactive-liganded ECR-ErbB4/NRG1β complex. Without ligand binding, the backbone root-mean-square deviation (rmsd) of ErbB4 showed no obvious fluctuations during the simulation time, indicating that the conformation of ErbB4 does not change dramatically throughout the 1 μs simulation (Figure 3A). Snapshots extracted from the MD trajectories also revealed that, during the simulation period,

dx.doi.org/10.1021/ja211941d | J. Am. Chem. Soc. 2012, 134, 6720−6731

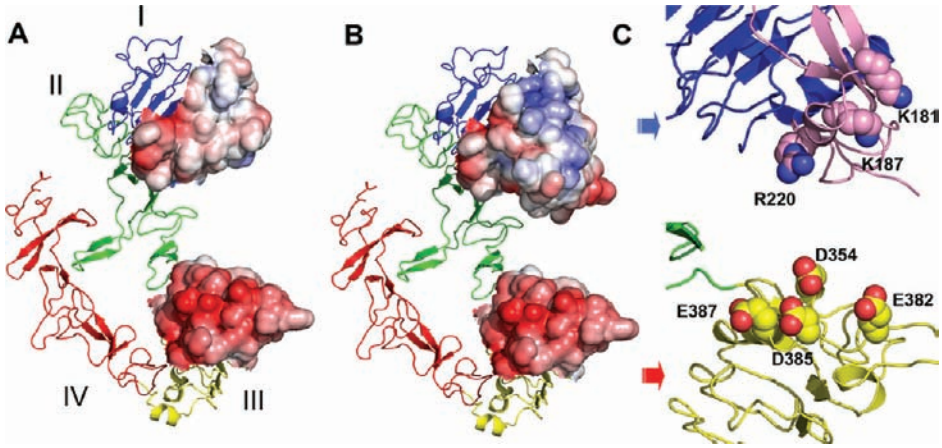

Figure 5. Electrostatic attraction between NRG1β and domain III of ECR-ErbB4. (A) Electrostatic potential surface of inactive ECR-ErbB4 in the absence of ligand NRG1β. (B) Electrostatic potential surface of ECR-ErbB4/NRG1β complex. (C) Positive charged residues of NRG1β and negative charged residues in domain III. Electrostatic charges for the electrostatic surface construction are contoured from red ($-5\ k_BT/e$) to blue ($+5\ k_BT/e$).

ErbB4 kept its architecture similar to the inactive starting structure (Figure 3B). This result also suggests that ErbB4 may not change from its inactive state to the active state spontaneously, implying that ligand binding is an important factor for the conformational transition. Indeed, upon NRG1β binding, ErbB4 underwent dramatic conformational changes during the simulation, as indicated in the rmsd profile (Figure 3A). The large-scale domain rearrangement is also demonstrated by the snapshots extracted from the MD trajectory, showing a conformational transition of ECR-ErbB4 from an inactive state to a conformation very close to the active state (called active-like state hereafter) (Figure 3C).

Although the transition took place continuously, the overall conformational rearrangement of ErbB4 can be roughly divided into three stages. The process begins with a stage in which the "tether" structure is maintained (0−350 ns). Some movements induced by NRG1β were seen at this stage. One motion is that domain I together with the ligand "rolls" over the surface of domain II like a wheel (Figure 4A). This motion decreases the cleft between domains I and II, while the contact surface between these two domains increases. The second motion is "bending" of domain II. Domain I together with the ligand undergoes a counterclockwise rotation around the axis near the tether, compelling domain II to bend into the plane of the paper as indicated by the maximum curvature of a fitted curve of the domain II "spine" (Figure 4B) (details of curvature calculation are described in the Methods section). All of these motions shorten the distance between the ligand and domain III (Figure 4C), making domain I and the ligand move toward domain III. Accordingly, the ligand is able to temporarily be in simultaneous touch with both of these domains at the end of this stage. The main obstacle for ErbB4 activation is the restriction of the domain II/IV tether,[60,61] which prevents domain I from moving closer to domain III. Apparently, the bending motion of domain II plays an important role in loosening the tether. As the bending of domain II increases, it can be assumed that its internal tension accumulatively increases. During this stage, the maximum curvature fluctuates with big amplitude. At about 230 ns, the bending reaches the maximum peak (Figure 4B, 230 ns snapshot). Afterward, it keeps fluctuating dramatically around 0.5 $Å^{-1}$ until 280 ns. At this time, the accumulated tension suddenly provokes domain II to rebound back to its unbent form, and the maximum curvature drops from 0.5 to 0.3 $Å^{-1}$ within ∼15 ns (280−295 ns) (Figure 4B). This sudden rebounding motion "injures" the "tether" and weakens the interaction of domain II/IV as indicated by the snapshot at 295 ns (Figure 4B). Releasing the tension, domain II bends into the plane of the paper again, and the conformational transition process enters into the second stage. It should be noted that, in addition to the motions described above, the interaction between the ligand and domain II at this stage might be of significance in inducing the conformational change (Figure 3C), for their contact surface increases quickly (0−25 ns) and almost keeps at ∼120 $Å^2$ throughout the remaining time of the MD simulation (Figure 4A).

Stage 2 is very short, lasting only from ∼350 to 390 ns. Bending to another maximum peak at ∼375 ns, domain II quickly rebounds back, and the rebounding force totally disrupts the tether as indicated by the representative snapshot (Figure 4B, the 375 ns snapshot) and distance profile of the tether (Figure 4D). At the end of this stage, the tether is completely opened, and the ligand contacts both domains I and III steadily. ErbB4 undergoes a rapid conformational change in this stage (Figure 3C, the third structure); consequently, the rmsd value of backbone atoms jumps from ∼10 Å up to ∼17 Å (Figure 3A). Another typical phenomenon at this stage is that both the contact surfaces of domain I and the ligand with domain II are generally reduced (Figure 4A).

During the third period (390−1000 ns), the tether has completely dissociated. Without the restriction of the tether, the domains adjust their interaction to the favored style, while domains II and IV separate from each other quickly (Figure 4D), leading the whole molecule to adopt a more extended conformation (Figure 3C, the fourth structure). Fast conformational change upon tether releasing seems to be consistent with the previous conclusion that the tether is an obstacle for ErbB4 activation.[60,61] The major movement at this stage is the relative motion between the domain I/II pair and the domain III/IV pair. When we compare panels A and B of Figure 4, it can be seen that the contact surface of domain I with domain II correlates well with the maximum curvature at stages 1 and 2. However, such correlation disappears at stage 3.

dx.doi.org/10.1021/ja211941d | J. Am. Chem. Soc. 2012, 134, 6720−6731

Although the 1 μs MD simulation on liganded ECR-ErbB4 did not reach the fully active conformation, the active-like conformation obtained should be an important state in the conformational transition pathway of the ECR-ErbB4/NRG1β complex as will be discussed below. Analysis of the two MD trajectories for the unliganded and liganded ErbB4 reveals some interesting differences that are indicative of the significant role played by the ligand in inducing conformational changes of the ErbB4 receptor.

Electrostatic Interaction Drives the Conformational Transition of ErbB4. We have addressed the role of NRG1β in inducing the conformational transition of ErbB4. What is the driving force triggering this conformational change? The gap between domains I and III of ErbB4 without ligand binding is about 60 Å in the crystal structure.[28] After NRG1β binding to domain I, the gap decreases to ~30 Å, still not allowing NRG1β to directly contact domain III. The electrostatic potential surfaces indicate that the surface of NRG1β facing the gap has a positively charged patch composed mainly of K181, K187, and R220, which was not seen in domain I of the unliganded ECR-ErbB4 (Figure 5A,B). The surface of domain III facing the gap has a negatively charged patch composed of D354, E382, D385, and E387 (Figure 5C). This suggests that an electrostatic interaction between domain III and NRG1β might be the driving force that pulls domains I and III together. To test this idea, we performed an additional simulation experiment. The surface properties of NRG1β were changed by substituting the three positively charged residues K181, K187, and R220 by negatively charged glutamates. Accordingly, the originally positively charged patch on NRG1β adopted a negative charge, leading to the repulsion of the negatively charged patch on domain III (Figure S1A in the Supporting Information). It can be deduced that this mutant of NRG1β would not be able to trigger the domain I movement toward domain III. Indeed, a 120 ns MD simulation of the ECR-ErbB4 complex with the NRG1β mutant showed that the distance between domain III and the ligand did not show the decreasing tendency seen in the case of the complex of ECR-ErbB4 with wild-type NRG1β (Figure S1B). This result demonstrates the importance of the electrostatic interaction between NRG1β and domain III in the conformational change of ErbB4. We propose that the electrostatic attraction as a driving force for conformational change might be a common phenomenon in the entire ErbB family. Upon inspection of the crystal structure of the inactive ECR-ErbB1/EGF complex,[29] we found that similar electrostatic interaction exists between EGF and domain III of ECR-ErbB1 (Figure S1C).

Dynamics of the Interface between Domains II and III. The X-ray structures available for ErbB family members imply that the major conformational difference between the inactive and active states lies in the relative orientation of the four domains.[25,27,28,32,33,35] Indeed, our MD simulations suggest that the structure of each domain per se is not subject to change as indicated by rmsd profiles (Figure S2A). The conformational change arises mainly from the dynamics of loops connecting these domains, in particular, of the U-shape loop between domains II and III. This loop functions as a hinge for the relative motion between the domain I/II pair and the domain III/IV pair. In the inactive state, domain II interacts with domain III through a salt bridge between D328 on the U-shaped loop and R396 on domain III (Figure 6A). Along with the conformational transition, this salt bridge is becoming weaker and is completely abolished at ~400 ns, as indicated by

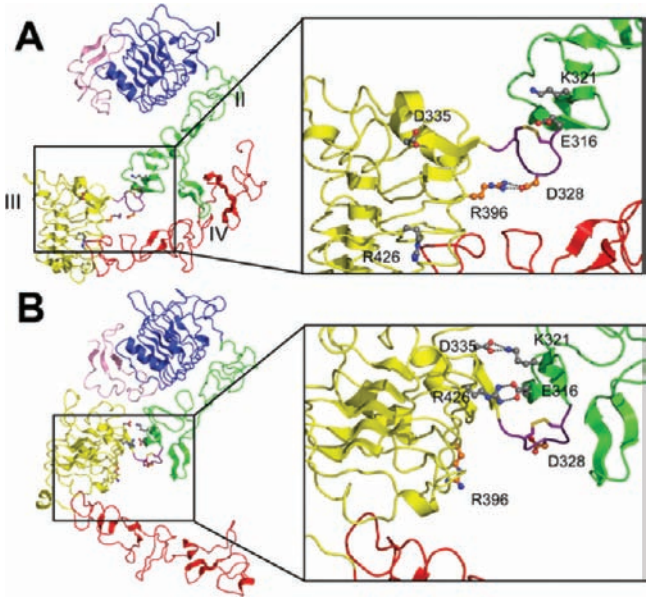

Figure 6. Dynamics of the interface between domains II and III. (A) Snapshot of ECR-ErbB4/NRG1β complex at 0 ns. The U-shaped loop (colored in purple) points to domain III, with the salt bridge formed by D328 and R396 (colored in orange) stabilizing this conformation. (B) Snapshot of ECR-ErbB4/NRG1β complex at 800 ns. The U-shaped loop is far from domain III. Domains II and III are close to each other, whereas salt bridges are formed by K321 and D335, as well as by E316 and R426 (colored in gray). NRG1β and domains I–IV are colored in pink, blue, green, yellow, and red, respectively.

the time dependence of the salt bridge distance (Figure S2B). Meanwhile, two new salt bridges gradually form between K321 on domain II and D335 on domain III and between E316 on domain II and R426 on domain III (Figure 6B), and after about 700 ns, these two interactions finally become strong hydrogen-bonding interactions (Figure S2B). These new hydrogen bonds enhance the interaction between domains II and III, stabilizing the active-like conformation of ErbB4.

Relative Motions between the Domains. To identify the most significant motions of ErbB4, principal component analysis (PCA) was carried out on the MD trajectory of the ECR-ErbB4/NRG1β complex. The first two principal components account for 70.5 and 9.3% of the overall motions. The first component (PC1) consists of several motions (Figure 7A): as a rigid body, the domain I/II pair undergoes a clockwise rotation out of the plane of the paper, domain III rotates counterclockwise out of the plane of the paper, and domain IV swings down and rotates into the paper in a direction opposite to domain III. These motions lead to a break of the tether, thereby enlarging the distance between the domains II and IV. Indeed, the projection of the trajectory on PC1 is highly correlated with the distance profile between the COMs of domains II and IV, with a correlation coefficient of 0.98 (Figure S3A). The second principal component (PC2) mainly corresponds to the opening rotation between the domain I/II pair and the domain III/IV pair with respect to the central hinge connecting them (Figure 7B). From the top, we can see that the domain I/II pair together with the ligand rotates clockwise, whereas the domain III/IV pair rotates counterclockwise. The profile of the cleft angle between these two pairs (defined by the vector connecting the COMs of domains II and I and the vector linking the COMs of domains III and IV)

dx.doi.org/10.1021/ja211941d | J. Am. Chem. Soc. 2012, 134, 6720–6731

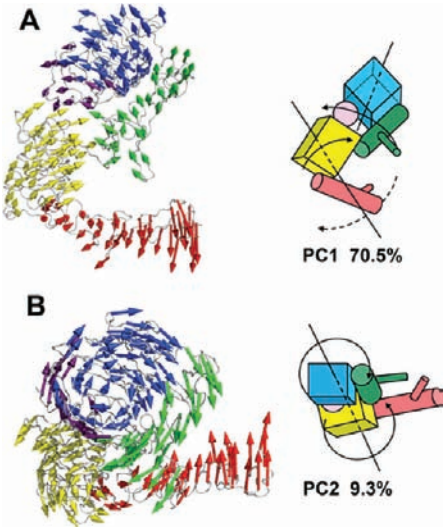

Figure 7. Collective motions obtained by principal component analysis (PCA) on the simulation trajectory of ECR-ErbB4/NRG1β complex. (A) Motions corresponding to the PC1, which accounts for ~70.5% of the total movements. (B) Motions corresponding to the PC2, which accounts for ~9.3% of the total movements.

agrees well with the PC2 movement, showing a correlation coefficient of −0.58 (Figure S3B).

Energy Landscape of the Conformational Transition. Our molecular dynamics simulation of ECR-ErbB4/NRG1β has addressed the large-scale conformational transition from the inactive state of ErbB4 to an active-like state. This 1 μs MD trajectory contains a broad range of conformations sampled around the configuration space, thereby providing abundant information for an energy landscape analysis for the conformational transition. According to the above principal component analysis, we have obtained two major motions associated with the conformational change of ErbB4; one is the separation of domains II and IV, and another is the opening rotation of the domain I/II pair with respect to the domain III/IV pair. Accordingly, during the energy landscape calculation, we used the distance between the COMs of domains II and IV and the cleft angle between the domain I/II pair and the domain III/IV pair as two reaction coordinates. The details of the energy profile calculation along the reaction coordinates are described in the Methods section.

The estimated energy landscape of the ECR-ErbB4/NRG1β complex corresponding to the two reaction coordinates is shown in Figure 8A. The energy landscape consists of two deep wells and a shallow one. The first deep well is mainly relevant to the conformations of stage 1 (0−350 ns) of the ErbB4/NRG1β complex conformational transition. Interestingly, mapping the conformations to the surface of the first deep well, we found that the starting structure is located halfway up the wall bordering the first well. Along with the conformational change, the ErbB4/NRG1β complex moves down to the first energy minimum. Afterward, it climbs up along the wall and reaches the second shallow well by passing over an energy barrier of ~2.7 kcal/mol. This calculation result is consistent with previous experiments showing that the tether of ErbB1 contributes 1−2 kcal/mol to the stabilization of the tethered state.[29,36] The second well corresponds to stage 2 of the ErbB4/NRG1β complex conformational transition. In agreement with the time scale (Figure 3A), ErbB4 stays in this well

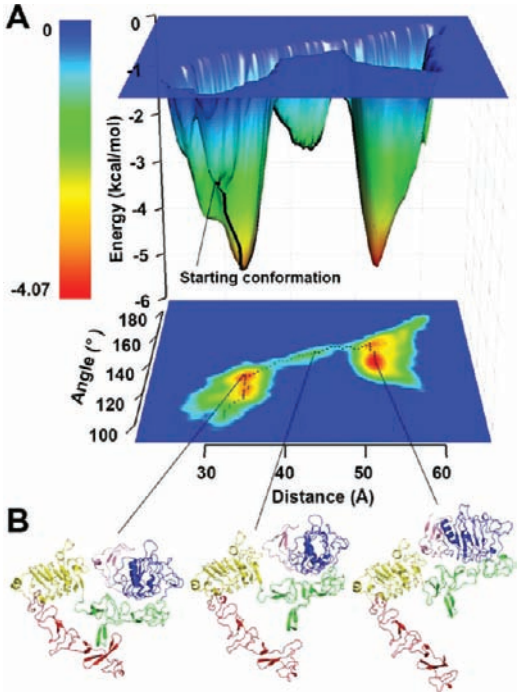

Figure 8. Energy landscape for the conformational transition of ECR-ErbB4/NRG1β complex. (A) Energy surface and its 2D contour map. The minimum energy pathway for the conformational change is shown by the black curve on the energy surface and the dashed line on the 2D contour map. Reaction coordinates are defined according to two indices: the COM distance between domains II and IV; the cleft angle of the domain I/II pair and the domain III/IV pair. These two indices are highly correlated with PC1 and PC2 obtained from PCA. (B) Typical conformations of energy minima.

shortly and then crosses over a low energy barrier (~1 kcal/mol) and moves downhill to the bottom of the third well, so as to reach the active-like state.

By going back from the energy landscape to the conformations of the MD trajectory, we can address some interesting phenomena. Structures around the bottom of the first well should be local minima (Figure 8B, first structure). Although such kinds of structures have not been experimentally obtained for ECR-ErbB4/NRG1β, a similar structure for the ECR-ErbB1/EGF complex has been determined by X-ray crystallographic technology[29] (Figure 1B) (PDB code: 1NQL). Superposition of the first local energy minimum structure of the ErbB4/NRG1β complex with the crystal structure of ErbB1/EGF complex shows only a small backbone rmsd value (4.1 Å) (Figure S4A). The structure of ErbB4/NRG1β at the bottom of the second well indicates that NRG1β is in contact with both domains I and III, and the tether has been loosened and is close to be broken (Figure 8B, second structure). The structure at the bottom of the third energy well has the domain II/IV tether completely unlocked, and the whole molecule adopts an extended active-like conformation (Figure 8B, third structure). Although the active-like structure is not as fully extended as the liganded-active state in crystal structure[35] (rmsd ~14.5 Å), the overall arrangements of domains are similar, and on the basis of the superimposition of the two structures, we conclude that the active-like structure still needs a rotation of ~80° around the hinge region between domains II and III to reach the fully activated conformation (Figure S4B).

dx.doi.org/10.1021/ja211941d | J. Am. Chem. Soc. 2012, 134, 6720−6731

DISCUSSION

In this study, we have investigated the dynamics of the extracellular region (ECR) of ErbB4 by using MD simulations and gained some insights into the activation mechanism of ErbB4 at the atomic level. Two 1 μs MD simulations have been performed on the crystal structure of ECR-ErbB4 and a model of the ECR-ErbB4/NRG1β complex. These MD simulations are much longer than other MD simulations carried out to date on ECRs of ErbBs.[62,63] The results indicate that long-time simulations are necessary in order to gain comprehensive insight into the conformational transition of ErbB4 and corresponding energy landscape (Figures 3 and 7).

One of the major findings of this study is that the simulation results provide direct evidence for the details of ErbB4 activation. We derived an activation process from the inactive ErbB4/NRG1β (with the ligand exclusively binding to domain I) to the untethered active-like conformation. In general, the overall conformational transition consists of three stages. The first stage concerns mainly accumulative motions. Induced by the electrostatic interaction of NRG1β with domain III, domain I of ErbB4 moves to domain III through two motions: domain I together with NRG1β rolling and domain II bending. Stage 2 is a short-term process that mainly concerns the loosening of the domain II/IV tether, making domain II depart from domain IV. During the third stage, the tether is completely dissociated, and domains II and IV separate from each other quickly (Figure 4D), leading the whole molecule to adopt a more extended conformation.

The bending motion of domain II at stages 1 and 2 plays an important role in disrupting the tether interaction. To quantitatively describe the bending motion, we formulated an equation to calculate the backbone curvature of domain II. The result indicates that domain II undergoes a remarkable bending vibration in the time range between 100 and 390 ns (Figure 4B). This bending and rebounding motion gradually disrupts the tether interaction (Figures 3C and 4B). So far, a role of domain II bending has been suggested to contribute to the dimerization of ErbB4 and other ErbBs. Dawson et al. proposed that ligand binding could impose a precise "bend" on domain II, which might be required to allow the multiple contact sites to effectively cooperate with the dimerization arm in driving ErbB's high-affinity dimerization.[64] It was also suggested by Lemmon et al. that, during the dimerization of ErbBs, different ligands might stabilize different degrees of domain II curvature to determine heterodimerization specificity.[61] The present MD simulation study reveals another possible role of domain II bending in ErbB4 activation: to loosen and interrupt the tether interaction between domains II and IV so as to help ECR-ErbB4 to overcome the main obstacle in activation.

Another important implication of our study is the role of the ligand NRG1β in the conformational transition of ErbB4. It is still unclear how exactly the ligand causes the activation and dimerization of the receptor, in particular, whether it takes effect through actively inducing the conformational changes needed for dimerization or just through stabilizing the extended configuration and thereby changing the pre-existed tethered/extended equilibrium.[36] Our MD simulations demonstrate that the conformation of unliganded ErbB4 is relatively stable during the 1 μs simulation time, whereas the receptor undergoes dramatic conformational changes upon NRG1β binding, suggesting that ligand binding is indeed the active inducing force for the conformational transition and subsequent dimerization. Our simulations also reveal that NRG1β binds to domain I of ErbB4 before it initiates the conformational change, and the electrostatic interaction between NRG1β and domain III of ECR-ErbB4 is the original driving force to trigger this conformational transition.

The abundant conformations obtained in the MD simulations provide an opportunity to explore the energetic properties of ErbB4 activation. On the basis of the PCA results and motion analysis, we constructed a rough energy landscape corresponding to the conformational change of ErbB4/NRG1β (Figure 8). Consistent with the three stages for conformational change (Figure 3), the energy landscape of the ErbB4/NRG1β complex composes of three energy minimum states. Interestingly, the conformation at the bottom of the first well does not correspond to the starting structure of the inactive ErbB4, as determined by X-ray crystallography.[25] Although this conformation has not been detected experimentally, some support for its existence comes from the X-ray crystal structure of the inactive ErbB1/EGF complex (PDB code: 1NQL).[29] This structure is thought to be in a "half-deactivated" state in which interactions between the ligand and domain III are disrupted, and EGF is supposed to dissociate rapidly from domain I in vivo.[29] The ErbB4/NRG1β conformation at the first well agrees well with the crystal structure of the inactive ErbB1/EGF complex, indicating that this state might be a common state for the ErbB family members and also important on the ligand-induced activation pathway. The structure in the third well is similar in the architecture to the active state (Figure S4B). Although the 1 μs MD simulation did not reach the fully active state of ErbB4, the energy minimum structure (active-like structure) in the third well should also be an important state for ErbB4. We deduce that this active-like conformation might be a "pre-state" for ErbB4 dimerization. Most possibly, other driving forces, perhaps induced by the other monomer of the receptor, are necessary to obtain the active conformation. From the energy landscape, we estimated the main energy barrier for tether opening of ErbB4. The calculated value of ~2.7 kcal/mol is very close to the experimental finding of 1−2 kcal/mol in the case of ErbB1.[29,36] This result verifies indirectly the reliability of our simulation results.

On the basis of our MD simulation results and analyses, we propose an atomic mechanism for the ligand-induced activation of ErbB4, as indicated in Figure 9. Initially, ligands such as NRG1β bind to domain I of ECR-ErbB4. Electrostatic interaction between the ligand and domain III initiates a series of domain motions (Figure 9A). Triggered by these motions, domain II undergoes a bending vibration. The "elastic force" causes domain II rebounding, which ruptures the tether interaction between domains II and IV (Figure 9B). Abolishment of the domain II/IV tether is the key step for the whole conformational change and further activation of the receptor.[32,56] Afterward, ErbB4 moves smoothly to an active-like state (Figure 9C). Finally, driven by other forces, including those induced by the other active-like monomer, ErbB4 adjusts the configuration and future participates in forming the dimer (Figure 9D).

Additionally, this study also provides some clues for drug discovery targeting ErbB4 or other ErbBs. As mentioned in the Introduction, ErbBs are important drug targets, which are associated with many diseases such as schizophrenia, heart failure, and several cancers.[6−10,17−22] Similar to the drug discovery efforts against other kinases, much attention has been devoted to the cytoplasmic kinase domain of ErbBs as a drug

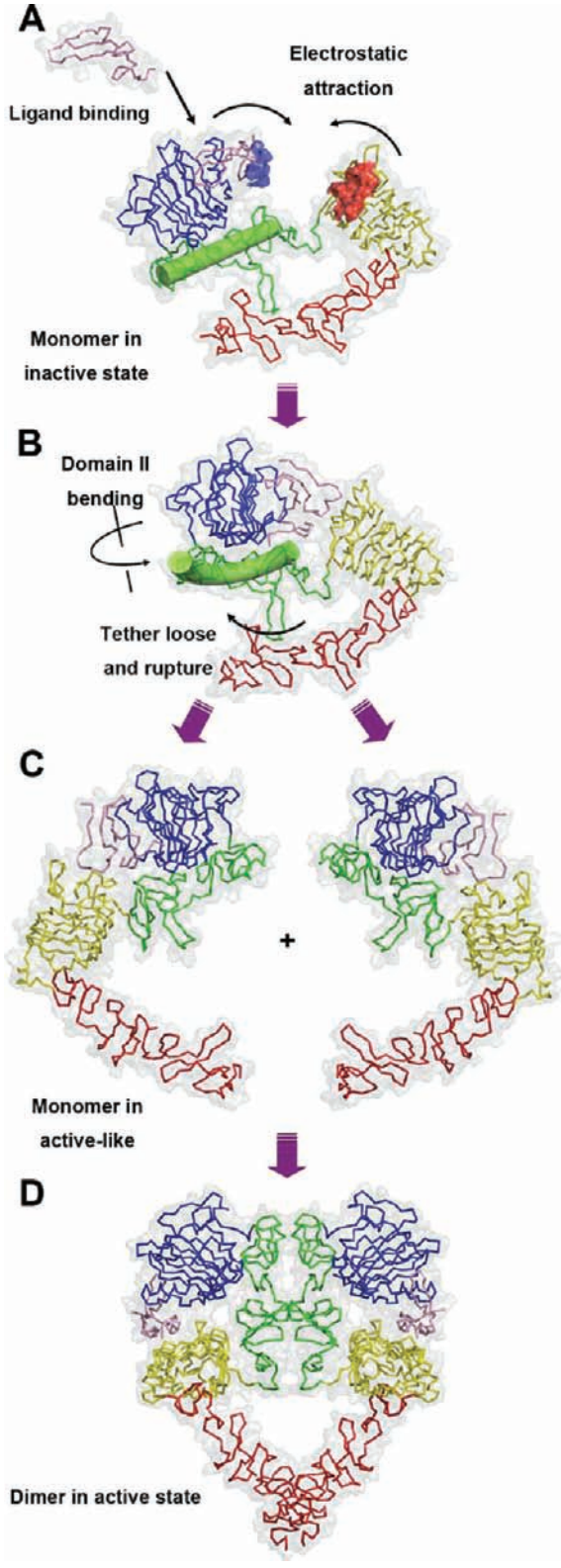

Figure 9. Detailed ligand-induced activation mechanism of ECR-ErbB4. The ligand initially binds to domain I of the ECR-ErbB4 and then triggers a series of motions due to the electrostatic attraction between the ligand and domain III (A). Induced by the domain rearrangement, domain II undergoes a bending and rebounding vibration, which loosens and finally ruptures the domain II/IV tether (B). After abolishment of tether, ECR-ErbB4 moves quickly to an active-like state (C). Two active-like state monomers alter the conformation and finally form the active dimer (D).

target.[65−68] Because of the high structural similarity of the kinase domain in different kinases, selectivity of the resulting inhibitors is far from satisfactory. Recently, the extracellular region of ErbB4 has been appreciated in drug discovery.[69,70] Modification of the endogenous ligands of ErbB4 or other ErbBs may be a good approach to discovery of new biological drugs. Our simulation indicates that neutralizing the positively charged residues on the surface of NRG1β could stabilize the ECR of ErbB4 in its inactive state (Figure S1). Such NRG1β mutants could be tested as drug candidates for the treatment of cancers or other diseases related to ErbB4's abnormal signaling.

■ CONCLUSION

In summary, the present study casts new insights into the activation of ErbB4 at the atomic level by using 1 μs conventional MD simulations, which allows for the following conclusions:

1. Ligand (NRG1β) binding is the active inducing force for the conformational transition and further dimerization of ErbB4. The free ligand initially binds to domain I of ErbB4, and the electrostatic attraction between the ligand and domain III might pull domains I and III to move together, thereby driving the conformational transition of ErbB4.

2. Induced by ligand binding, domain I of ErbB4 gets close to domain III through two motions: the rolling of domain I over domain II and the bending of domain II, which result in the rupture of the domain II/IV tether (a major obstacle in activation process) and further the tremendous domain rearrangement. In particular, the bending motion of domain II plays a pivotal role in disrupting the tether.

3. The agreement between the estimated energy barrier for the tether opening (~2.7 kcal/mol) and the experimental value reported for ErbB1 (1−2 kcal/mol) implies the reasonability of the pathway for the conformational transition of ErbB4. The energy landscape analysis for the conformational change captured a stable state in local minimum for ErbB4, which is very similar to the X-ray crystal structure of ECR-ErbB1/EGF complex. This might be useful information for further experimental studies.

4. The proposed atomic mechanism for the ligand-induced activation of ErbB4 also provides clues for studying the activation mechanism of other ErbBs and for designing new therapies targeting these receptors.

■ ASSOCIATED CONTENT

Supporting Information

More detailed analysis of the conformational transition of ECR-ErbB4/NRG1β. Complete ref 10 is also listed in Supporting Information. This material is available free of charge via the Internet at http://pubs.acs.org.

■ AUTHOR INFORMATION

Corresponding Author

hljiang@mail.shcnc.ac.cn; hy_yang@mail.shcnc.ac.cn

Notes

The authors declare no competing financial interest.

■ ACKNOWLEDGMENTS

This work was supported by the State Key Program of Basic Research of China (2009CB918502), the National Natural Science Foundation of China (20721003 and 20720102040),

and the National S&T Major Project (2009ZX09501-001), and '100 Talents Project' of CAS (to YX). Computational resources were supported by the National Supercomputing Center in Tianjin (Tianhe-1), Shanghai Supercomputer Center and the Computer Network Information Center of the Chinese Academy of Sciences. We thank Prof. Rolf Hilgenfeld of University of Lübeck for his help in revising English usage.

REFERENCES

(1) Olayioye, M. A.; Neve, R. M.; Lane, H. A.; Hynes, N. E. *EMBO J.* **2000**, *19*, 3159−3167.
(2) Warren, C. M.; Landgraf, R. *Cell Signal* **2006**, *18*, 923−933.
(3) Lurje, G.; Lenz, H. J. *Oncology* **2009**, *77*, 400−410.
(4) Mendelsohn, J.; Baselga, J. *Oncogene* **2000**, *19*, 6550−6565.
(5) Gassmann, M.; Casagranda, F.; Orioli, D.; Simon, H.; Lai, C.; Klein, R.; Lemke, G. *Nature* **1995**, *378*, 390−394.
(6) Zhao, Y. Y.; Sawyer, D. R.; Baliga, R. R.; Opel, D. J.; Han, X.; Marchionni, M. A.; Kelly, R. A. *J. Biol. Chem.* **1998**, *273*, 10261−10269.
(7) Bersell, K.; Arab, S.; Haring, B.; Kuhn, B. *Cell* **2009**, *138*, 257−270.
(8) Mei, L.; Xiong, W. C. *Nat. Rev. Neurosci.* **2008**, *9*, 437−452.
(9) Benzel, I.; Bansal, A.; Browning, B. L.; Galwey, N. W.; Maycox, P. R.; McGinnis, R.; Smart, D.; St. Clair, D.; Yates, P.; Purvis, I. *Behav. Brain Funct.* **2007**, *3*, 31.
(10) Norton, N.; et al. *Am. J. Med. Genet., Part B* **2006**, *141B*, 96−101.
(11) Xu, Y.; Li, X.; Liu, X.; Zhou, M. *Adv. Pharmacol.* **2010**, *59*, 31−51.
(12) Aqeilan, R. I.; Donati, V.; Gaudio, E.; Nicoloso, M. S.; Sundvall, M.; Korhonen, A.; Lundin, J.; Isola, J.; Sudol, M.; Joensuu, H.; Croce, C. M.; Elenius, K. *Cancer Res.* **2007**, *67*, 9330−9336.
(13) Naresh, A.; Long, W.; Vidal, G. A.; Wimley, W. C.; Marrero, L.; Sartor, C. I.; Tovey, S.; Cooke, T. G.; Bartlett, J. M.; Jones, F. E. *Cancer Res.* **2006**, *66*, 6412−6420.
(14) Pitfield, S. E.; Bryant, I.; Penington, D. J.; Park, G.; Riese, D. J. II. *Oncol. Res.* **2006**, *16*, 179−193.
(15) Williams, E. E.; Trout, L. J.; Gallo, R. M.; Pitfield, S. E.; Bryant, I.; Penington, D. J.; Riese, D. J. II. *Cancer Lett.* **2003**, *192*, 67−74.
(16) Kew, T. Y.; Bell, J. A.; Pinder, S. E.; Denley, H.; Srinivasan, R.; Gullick, W. J.; Nicholson, R. I.; Blamey, R. W.; Ellis, I. O. *Br. J. Cancer* **2000**, *82*, 1163−1170.
(17) Tovey, S. M.; Witton, C. J.; Bartlett, J. M.; Stanton, P. D.; Reeves, J. R.; Cooke, T. G. *Breast Cancer Res.* **2004**, *6*, R246−R251.
(18) Mill, C. P.; Gettinger, K. L.; Riese, D. J. II. *Exp. Cell Res.* **2011**, *317*, 392−404.
(19) Maatta, J. A.; Sundvall, M.; Junttila, T. T.; Peri, L.; Laine, V. J.; Isola, J.; Egeblad, M.; Elenius, K. *Mol. Biol. Cell* **2006**, *17*, 67−79.
(20) Starr, A.; Greif, J.; Vexler, A.; Ashkenazy-Voghera, M.; Gladesh, V.; Rubin, C.; Kerber, G.; Marmor, S.; Lev-Ari, S.; Inbar, M.; Yarden, Y.; Ben-Yosef, R. *Int. J. Cancer* **2006**, *119*, 269−274.
(21) Tang, C. K.; Concepcion, X. Z.; Milan, M.; Gong, X.; Montgomery, E.; Lippman, M. E. *Cancer Res.* **1999**, *59*, 5315−5322.
(22) Zhu, Y.; Sullivan, L. L.; Nair, S. S.; Williams, C. C.; Pandey, A. K.; Marrero, L.; Vadlamudi, R. K.; Jones, F. E. *Cancer Res.* **2006**, *66*, 7991−7998.
(23) Lodge, A. J.; Anderson, J. J.; Gullick, W. J.; Haugk, B.; Leonard, R. C.; Angus, B. *J. Clin. Pathol.* **2003**, *56*, 300−304.
(24) Lazzara, M. J.; Lauffenburger, D. A. *Exp. Cell Res.* **2009**, *315*, 717−725.
(25) Bouyain, S.; Longo, P. A.; Li, S.; Ferguson, K. M.; Leahy, D. J. *Proc. Natl. Acad. Sci. U.S.A.* **2005**, *102*, 15024−15029.
(26) Plowman, G. D.; Green, J. M.; Culouscou, J. M.; Carlton, G. W.; Rothwell, V. M.; Buckley, S. *Nature* **1993**, *366*, 473−475.
(27) Li, S.; Schmitz, K. R.; Jeffrey, P. D.; Wiltzius, J. J.; Kussie, P.; Ferguson, K. M. *Cancer Cell* **2005**, *7*, 301−311.
(28) Cho, H. S.; Leahy, D. J. *Science* **2002**, *297*, 1330−1333.
(29) Ferguson, K. M.; Berger, M. B.; Mendrola, J. M.; Cho, H. S.; Leahy, D. J.; Lemmon, M. A. *Mol. Cell* **2003**, *11*, 507−517.
(30) Franklin, M. C.; Carey, K. D.; Vajdos, F. F.; Leahy, D. J.; de Vos, A. M.; Sliwkowski, M. X. *Cancer Cell* **2004**, *5*, 317−328.
(31) Fisher, R. D.; Ultsch, M.; Lingel, A.; Schaefer, G.; Shao, L.; Birtalan, S.; Sidhu, S. S.; Eigenbrot, C. *J. Mol. Biol.* **2010**, *402*, 217−229.
(32) Garrett, T. P.; McKern, N. M.; Lou, M.; Elleman, T. C.; Adams, T. E.; Lovrecz, G. O.; Zhu, H. J.; Walker, F.; Frenkel, M. J.; Hoyne, P. A.; Jorissen, R. N.; Nice, E. C.; Burgess, A. W.; Ward, C. W. *Cell* **2002**, *110*, 763−773.
(33) Ogiso, H.; Ishitani, R.; Nureki, O.; Fukai, S.; Yamanaka, M.; Kim, J. H.; Saito, K.; Sakamoto, A.; Inoue, M.; Shirouzu, M.; Yokoyama, S. *Cell* **2002**, *110*, 775−787.
(34) Dawson, J. P.; Bu, Z.; Lemmon, M. A. *Structure* **2007**, *15*, 942−954.
(35) Lu, C.; Mi, L. Z.; Grey, M. J.; Zhu, J.; Graef, E.; Yokoyama, S.; Springer, T. A. *Mol. Cell. Biol.* **2010**, *30*, 5432−5443.
(36) Burgess, A. W.; Cho, H. S.; Eigenbrot, C.; Ferguson, K. M.; Garrett, T. P.; Leahy, D. J.; Lemmon, M. A.; Sliwkowski, M. X.; Ward, C. W.; Yokoyama, S. *Mol. Cell* **2003**, *12*, 541−552.
(37) Jacobsen, N. E.; Abadi, N.; Sliwkowski, M. X.; Reilly, D.; Skelton, N. J.; Fairbrother, W. J. *Biochemistry* **1996**, *35*, 3402−3417.
(38) Luo, C.; Xu, L.; Zheng, S.; Luo, X.; Shen, J.; Jiang, H.; Liu, X.; Zhou, M. *Proteins* **2005**, *59*, 742−756.
(39) Hess, B.; Kutzner, C.; van der Spoel, D.; Lindahl, E. *J. Chem. Theory Comput.* **2008**, *4*, 435−447.
(40) van der Spoel, D.; Lindahl, E.; Hess, B.; Groenhof, G.; Mark, A. E.; Berendsen, H. J. *J. Comput. Chem.* **2005**, *26*, 1701−1718.
(41) Duan, Y.; Wu, C.; Chowdhury, S.; Lee, M. C.; Xiong, G.; Zhang, W.; Yang, R.; Cieplak, P.; Luo, R.; Lee, T.; Caldwell, J.; Wang, J.; Kollman, P. *J. Comput. Chem.* **2003**, *24*, 1999−2012.
(42) Lee, M. C.; Duan, Y. *Proteins* **2004**, *55*, 620−634.
(43) Wang, J. M.; Wolf, R. M.; Caldwell, J. W.; Kollman, P. A.; Case, D. A. *J. Comput. Chem.* **2004**, *25*, 1157−1174.
(44) Jorgensen, W. L.; Chandrasekhar, J.; Madura, J. D.; Impey, R. W.; Klein, M. L. *J. Chem. Phys.* **1983**, *79*, 926−935.
(45) Berendsen, H. J. C.; Postma, J. P. M; van Gunsteren, W. F.; DiNola, A.; Haak, J. R. *J. Chem. Phys.* **1984**, *81*, 3684−3690.
(46) Darden, T.; York, D.; Pedersen, L. *J. Chem. Phys.* **1993**, *98*, 10089−10092.
(47) Essmann, U.; Perera, L.; Berkowitz, M. L.; Darden, T.; Lee, H.; Pedersen, L. G. *J. Chem. Phys.* **1995**, *103*, 8577−8592.
(48) Hess, B.; Bekker, B.; Berendsen, H. J. C.; Fraaije, J. G. E. M. *J. Comput. Chem.* **1997**, *18*, 1463−1472.
(49) Dolinsky, T. J.; Czodrowski, P.; Li, H.; Nielsen, J. E.; Jensen, J. H.; Klebe, G.; Baker, N. A. *Nucleic Acids Res.* **2007**, *35*, W522−W525.
(50) Dolinsky, T. J.; Nielsen, J. E.; McCammon, J. A.; Baker, N. A. *Nucleic Acids Res.* **2004**, *32*, W665−W667.
(51) Baker, N. A.; Sept, D.; Joseph, S.; Holst, M. J.; McCammon, J. A. *Proc. Natl. Acad. Sci. U.S.A.* **2001**, *98*, 10037−10041.
(52) Delano, W. L. *The PyMOL User's Manual*; DeLano Scientific LCC: San Carlos, CA, 2002.
(53) Amadei, A.; Linssen, A. B.; Berendsen, H. J. *Proteins* **1993**, *17*, 412−425.
(54) Papaleo, E.; Mereghetti, P.; Fantucci, P.; Grandori, R.; De Gioia, L. *J. Mol. Graphics Modell.* **2009**, *27*, 889−899.
(55) Zhou, R.; Berne, B. J.; Germain, R. *Proc. Natl. Acad. Sci. U.S.A.* **2001**, *98*, 14931−14936.
(56) Garcia, A. E.; Sanbonmatsu, K. Y. *Proteins* **2001**, *42*, 345−354.
(57) Fields Development Team (2006). Fields: Tools for Spatial Data. National Center for Atmospheric Research, Boulder, CO; http://www.cgd.ucar.edu/Software/Fields.
(58) R Development Core Team (2008). R: A language and environment for statistical computing. R Foundation for Statistical Computing, Vienna, Austria; ISBN3-900051-07-0, http://www.R-project.org.

(59) Nenadic, O.; Adler, D.; Zucchini, W. In CARME 2003: International Conference on Correspondence Analysis and Related Methods Barcelona, Spain, 2003.
(60) Gilmore, J. L.; Riese, D. J. II. *Oncol. Res.* **2004**, *14*, 589−602.
(61) Lemmon, M. A. *Exp. Cell Res.* **2009**, *315*, 638−648.
(62) Kastner, J.; Loeffler, H. H.; Roberts, S. K.; Martin-Fernandez, M. L.; Winn, M. D. *J. Struct. Biol.* **2009**, *167*, 117−128.
(63) Zhang, Z.; Wriggers, W. *Biochemistry* **2010**, *50*, 2144−2156.
(64) Dawson, J. P.; Berger, M. B.; Lin, C. C.; Schlessinger, J.; Lemmon, M. A.; Ferguson, K. M. *Mol. Cell. Biol.* **2005**, *25*, 7734−7742.
(65) Morabito, A.; Piccirillo, M. C.; Falasconi, F.; De Feo, G.; Del Giudice, A.; Bryce, J.; Di Maio, M.; De Maio, E.; Normanno, N.; Perrone, F. *Oncologist* **2009**, *14*, 378−390.
(66) Nelson, M. H.; Dolder, C. R. *Ann. Pharmacother.* **2006**, *40*, 261−269.
(67) Bonomi, P. *Expert Opin. Invest. Drugs* **2003**, *12*, 1395−1401.
(68) Barker, A. J.; Gibson, K. H.; Grundy, W.; Godfrey, A. A.; Barlow, J. J.; Healy, M. P.; Woodburn, J. R.; Ashton, S. E.; Curry, B. J.; Scarlett, L.; Henthorn, L.; Richards, L. *Bioorg. Med. Chem. Lett.* **2001**, *11*, 1911−1914.
(69) Gao, R.; Zhang, J.; Cheng, L.; Wu, X.; Dong, W.; Yang, X.; Li, T.; Liu, X.; Xu, Y.; Li, X.; Zhou, M. *J. Am. Coll. Cardiol.* **2010**, *55*, 1907−1914.
(70) Schmitz, K. R.; Ferguson, K. M. *Exp. Cell Res.* **2009**, *315*, 659−670.